IMPACT OF MITOCHONDRIAL TRANSCRIPTION FACTOR A-DNA BINDING ON THE ENZYMATIC ABILITY OF ALKYLADENINE DNA GLYCOSYLASE

By

Yuvraj Singh

A capstone project submitted for Graduation with University Honors

May 12, 2023

University Honors

University of California, Riverside

APPROVED

Dr. Linlin Zhao

Department of Chemistry

Dr. Richard Cardullo, Howard H Hays Jr. Chair

University Honors

ABSTRACT

Mitochondria are crucial organelles within eukaryotes responsible for producing energy, signaling pathways, and biosynthesis within the cell. Mitochondrial DNA (mtDNA) encodes for a complex set of proteins essential to the constant function of the cell. Proteins such as helicase twinkle, DNA polymerase (poly γ), mitochondrial single-stranded binding protein (mtSSB), and mitochondrial transcription factor A (TFAM) are responsible for the replication and maintenance of mtDNA. Alkyladenine DNA glycosylase (AAG) is an important DNA repair enzyme that localizes to both the nucleus and mitochondria and is responsible for removing damaged nucleobases within DNA. AAG targets modifications at the N7 position of guanine and N3 position of adenine, as well as those derived from reactive aldehydes such as 1, N4-ethenoadenine (εA) and 3,N4-ethonocytosine (εC) mutations. TFAM is a major mtDNA packaging protein which binds to the double-stranded mtDNA. The impact of shared localization of TFAM and AAG on mtDNA is explored in our study. In this study, we carried out steady-state kinetics assays, and stimulation assays, with hAAG (human alkyladenine DNA glycosylase) using a fluorescently labeled hypoxanthine/inosine-containing dsDNA. Reaction rates of AAG-catalyzed excision were compared with and without the presence of TFAM. By comparing the parameters, we can analyze the impact TFAM might have on the glycosylase activity of AAG. Data collected indicate that varied concentrations of TFAM play a stimulating, and inhibiting role when complex with dsDNA, suggesting multiple roles of TFAM in regulating DNA repair.

ACKNOWLEDGEMENTS

I would like to first thank my faculty mentor, Dr. Linlin Zhao for his considerable effort and time in mentoring me through my research and academics. Dr. Zhao's contributions to my professional development have allowed me to escalate my growth as a student in research. He created a nurturing environment that has allowed me to hone my skills in research, literature, and academia, which will impact me throughout my career.

I would also like to thank my graduate student mentor, Kathleen Urrutia, for her daily mentoring, and patience in helping me learn how to be a great enzymologist. Her constant care for my education has helped me truly learn the intricacies of competitive research in biochemistry. The skills that I have learned from observing her, and completing work under her supervision will stick with me as I continue my work in science.

Lastly, I want to acknowledge and thank the entirety of Zhao Lab for their altruism and love for teaching their juniors. Without the culmination of lessons and learning experiences, I gained from my peers, I would not have succeeded. I am grateful for the environment which they created, and I hope to replicate this in the future.

Table of Contents

INTRODUCTION

The mitochondria are essential organelles within eukaryotic organisms that regulate cellular metabolism, oxidative stress control, and can be involved with apoptosis (Atig et. al., 2009). Like the nuclear genome, mitochondria have their own unique Mitochondrial DNA (mtDNA). Human mtDNA is double-stranded and circular, weighing around 10^7 Daltons (Sharma et. al., 2019). This mtDNA encodes for the proteins responsible for energy production through the citric acid cycle, electron transport chain, and maintenance of the mtDNA. For example, mtDNA encodes 13 polypeptides for the oxidative phosphorylation complex (Sharma et. al, 2019). This mtDNA encodes for the proteins responsible for energy production through the citric acid cycle, electron transport chain, and maintenance of the mtDNA. Mitochondrial DNA is fragile, and prone to damage through a variety of forces including oxidative damage, alkylation, deamination, and much more (Zhang et. al., 2014). This damage can lead to mispairing, inhibition of transcription, and mutations, or cell death. It is characteristic of mtDNA to have a high rate of mutations (Atig et. al., 2009). Damage to the bases in DNA is repaired through a processive mechanism called the Base Excision Repair pathway. The cell has developed an intricate system of repair mechanisms that prevent or repair damaged DNA common in both nuclear and mitochondrial genomes. Base excision repair (BER) utilizes an enzyme, a glycosylase, to cut damaged DNA bases out of the genome, and in conjunction with its peer enzymes such as AP endonuclease, the mechanism repairs the DNA damage. The base excision repair pathway begins firstly with a glycosylase recognizing and removing a damaged base. This creates an abasic site (AP site) where an AP endonuclease (APE1) will then follow through and create a single-strand break. DNA polymerase will install the correct nucleotide based on the template strand (undamaged strand), and DNA ligase III will finish the repair by rejoining the strand. The sequential events of the base excision repair mechanism will be

completed, and the damaged base will have been repaired. DNA glycosylase's ability to identify and initiate the base excision repair pathway is essential to maintaining the integrity of mtDNA.

Alkyladenine DNA Glycosylase is one such glycosylase participating in the repair of damaged bases of mtDNA. Alkyladenine DNA Glycosylase (AAG) is a 33 kD monomeric protein that localizes to the mitochondria where it is an essential enzyme that targets damage at the N7 position of guanine and N3 position of adenine, and damage from reactive aldehydes such as 1, N4-ethenoadenine (εA) and 3, -N4-ethonocytosine (εC) mutations (Hedglin et. al, 2008). AAG participates in BER and examines the dsDNA for damaged bases before excising the base from the DNA strand leaving behind an abasic site. The protein, which localizes both in the nuclear and mitochondrial DNA regions, is one of the few glycosylases known to be able to excise alkylated purines (Kennedy et. al., 2019). AAG is able to complete this through a variety of selectivity filters ensuring correct excisions. AAG looks for unstable base pairs to excise, which, when combined with a catalytic mechanism using general acid catalysis ensures the excision of only purines. The remaining selectivity filter involves the use of unfavorable steric conditions of exocyclic amino groups of guanine and adenine to recognize any purines missing these conditions and target them (Hedglin et. al, 2008). Furthermore, research has found that AAG is able to bind to DNA and search at a minimum of 25 base pairs before the protein dissociates (Hedglin et. al, 2008). This allows for an extra redundancy factor to search for multiple damaged bases in a single-binding event. Furthermore, it also indicates that AAG participates in non-specific binding to undamaged bases. It is important to understand the function of how AAG completes its search for damaged bases as it is responsible for initiating a DNA repair mechanism essential to the survivability of the mitochondria. Another protein that is

essential for the integrity of mtDNA and localizes in the same region as AAG is mitochondrial transcription factor A (TFAM).

TFAM and AAG are both essential in the upkeep of mtDNA, and are often localized, and likely present together at the same time in the mitochondria. TFAM is a mitochondrial binding protein that plays an integral role in the stability, packaging, and replication of the mitochondrial genome. Usually binding at the promoter region, TFAM binds nonspecifically on mtDNA when condensing the genome. The structural function of TFAM involves wrapping mtDNA, and packaging it into nucleoid structures, resembling histones with the nuclear genome (Xu et. al., 2019). In terms of maintenance, TFAM is responsible for regulating mtDNA replication, and therefore maintaining an appropriate mtDNA copy number (Chandrasekaran et. al., 2019). Research by our lab, Zhao Lab, has shown that TFAM can also play a role in the degradation of abasic sites. In a paper, the lab found that binding of TFAM to an abasic site reduced the stability of the site significantly. The complex of TFAM and DNA bound at the abasic site was found to have a half-life which was 2 to 3 orders of magnitude shorter than it would have been for free DNA (Xu, et. al., 2019). Clearly, the impact that TFAM has on the maintenance and repair of mtDNA is significant. Therefore, it is important to understand the implications of both AAG and TFAM being present and localized in the mtDNA region.

In this project, we work to define the impact of TFAM binding to double-stranded DNA (dsDNA) will have on the glycosylase activity of AAG. It is important that AAG functions appropriately as the prolonged lifetime of abasic sites may lead to detrimental consequences for the mitochondria, and cells. Furthermore, neglect of DNA damage repair can be linked to the development of human disease. Glycosylase deficiencies and mutations inactivating glycosylase production have been reported in human cancers and metabolic pathogenesis for diseases such as

fatty liver and obesity (Sampath et. al, 2012). Therefore, it is valuable to study and understand if TFAM is indeed causing inhibition, any stimulation of AAG's glycosylase activity, or no effect.

Methodology

TFAM-AAG Assay. To understand the impact of one protein on the other, it was important to set up an assay which allows for the competition between the proteins and the binding of dsDNA. An assay competing AAG against TFAM complexed with dsDNA was used to understand if TFAM binding to dsDNA prior to the introduction of AAG would cause the stimulation of AAG product formation, and therefore, an increase in AAG glycosylase activity. The assay is set up in 0.6 µL microcentrifuge tubes. Two buffers, DNA reaction buffer, and protein dilution buffer are to be made prior to the start of the assay. The protein dilution buffer includes 50 mM HEPES pH 7.4, 100 mM NaCl, 0.1 mg/ml of BSA, 50% glycerol, 5 mM DTT, and miliq H2O. This buffer is used to dilute the stock protein down to the desired concentrations for the assay. The DNA reaction buffer contains 50 mM HEPES pH 7.4, 100 mM NaCl, 0.1 mg/ml of BSA, 1 mM EDTA, and 1 µM of duplex DNA. This buffer serves as the DNA carrying solution, and the solvent which will carry out the assay when TFAM and AAG are added. The duplex DNA being used in this experiment is the A3/13 oligo which is fluorescently labeled and contains hypoxanthine/inosine which serves as the damaged base for AAG and TFAM to bind. A3/13 is the combination of AAG-3: AAG-3-LSP-dI, and TFAM-13 which is the unlabeled complimentary strand to AAG-3 (/56FAM/TAACAGTCACCCCCC/ideoxyI/ACTAAC, and 5'-GTT AGT TGG GGG GTG ACT GTT A, respectively). The AAG-3 contains a 5'-FAM label. Before the assay is started, both proteins, AAG and TFAM, will need to be diluted down to the appropriate concentrations to use for the assay. Concentrations are confirmed via nanodrop machine, and Beer-Lambert law calculations using each protein's extinction coefficients (AAG:

25440 M^{-1} cm^{-1}; TFAM 35410 M^{-1} cm^{-1}). The Beer-Lambert equation is as follows: $A = \varepsilon bC$, where A is the absorbance, ε provides the molar absorptivity depending on the protein, *b* is the path length assumed usually as 1 cm, and C is the concentration of the protein. The nanodrop will provide absorbance values at wavelength of 280nm for each protein. The average of three readings is used to determine the concentrations of protein in dilution after the Beer-Lambert equations have been used. Depending on the number of points (concentrations) being tested for TFAM, the dilutions may vary. The assay must be completed at 37 °C for optimum enzyme kinetics conditions; therefore, a heat-block is used at the temperature. The assay will follow a time-table set-up to maximize binding of TFAM kinetic equilibrium before the addition of AAG. The experiment is ran for 35 minutes total, with quenching of the reaction beginning at the 35 minute mark. The assay will begin when the DNA is added to the heat-block for preheating before any protein is added to the reaction mixture.

Time (minutes. Seconds)		Time	
0.00		35.00	Quench 0.1
1.00	+ 0.1 ADD TFAM and DNA to HEAT		+ 0.2
1.30	+ 0.2		+ 0.3
2.00	+ 0.3		+ 0.5
2.30	+ 0.5		+ 0.6
3.00	+ 0.6		+ 0.8
3.30	+ 0.8		+ 1.0
4.00	+ 1.0		
4.30	+ TFAM to 0.1		
5.00	+ 0.2		
5.30	+ 0.3		
6.00	+ 0.5		
6.30	+ 0.6		
7.00	+ 0.8		
7.30	+ 1.0		
8.00	+ AAG to 0.1		
8.30	+ 0.2		
9.00	+ 0.3		
9.30	+ 0.5		
10.00	+ 0.6		
10.30	+ 0.8		
11.00	+ 1.0		

Figure 1. Sample Timetable to follow for the TFAM-AAG Assay.

TFAM is added first to the DNA reaction mixture so that it can reach kinetic equilibrium. AAG is added only after TFAM has been added to the DNA reaction mixture for all

concentrations of TFAM. Following a timetable such as figure 1, once AAG is added to all of the tubes, you must wait until the 35-minute mark to quench the reaction.

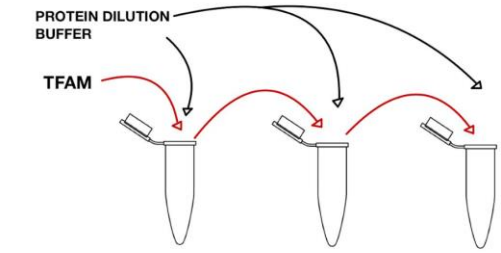

a.

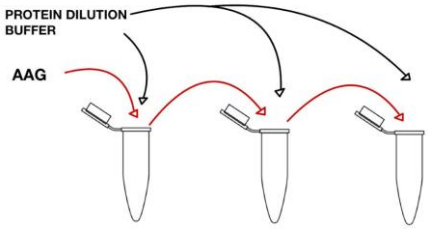

b.

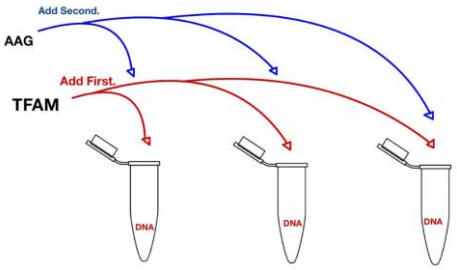

c.

Figure 2. Model of steps for assay. 2a. TFAM is diluted in a serial dilution. 2b. AAG is diluted in a serial dilution until desired concentration is reached. 2c. Steps to adding TFAM and AAG into the running reaction. TFAM is added first to all points, followed by AAG.

The reaction is quenched with 0.4 M NaOH. NaOH is what induces the single-stranded break in the DNA. Quenching would allow product formation by AAG. Once quenching is complete, the samples are incubated at 70 °C for 15 minutes before the addition of a stop solution including formamide and subsequent addition of HCl. The denaturing step involves 15 minutes at 95 °C before the samples are spun down in a centrifuge for 1 minute and prepped for loading into a gel. Throughout this process, mixing of the reaction is required at each step to ensure a homologous reaction.

Visualizing using Mini-Gel Denaturing Page. The gel used to visualize the results is a 16% Urea-PAGE Gel. The mini gel is constructed using Bio-Rad material at 0.75 mm thickness. The 16% gel allows for the pore sizes in the gel to be relatively large, and therefore allows for completion of a gel run at a quicker time without sacrificing quality. The larger pore size allows

for molecules of product and DNA to pass through the gel at a relatively faster rate than compared to a higher percentage gel. The gel is run at 200 volts for 45 minutes before it can be imaged. As the reaction mixture includes fluorescently labeled DNA, there are no staining and detaining steps. The imaging is done by a typhoon imager with FAM settings as it is the fluorescent label, and 1D-gel analysis is conducted. Once the gel's data has been collected, the data is translated into a graph to visualize the product formation using Graph Pad Prism.

Results

Initial steps in the assay were to optimize the assay for a specific concentration range. Therefore, the first experiment was completed using a range of 0.1 µM to 2.0 µM of TFAM. This would allow for a general understanding of what may be occurring with TFAM and AAG interactions. This optimization assay was completed with two different concentrations of AAG as well. This was to determine if different concentrations of AAG would be impacted in the same way when competing against TFAM. It was seen through this assay that in lower concentrations of TFAM, not only is there no inhibition of AAG, but rather an increase in the product formed is seen (Figure 3). When examining the gel image, there is a clear increase in product formation, and therefore glycosylase activity in the smaller concentrations (0.2. 0.5 µM) versus the larger concentrations (1.0, 2.0 µM). Based on just a visual test, the darker bands on the gel image for each lane indicate how much product was formed. Compared to the 200 nM assay, the 400 nM assay was producing much more product. Both indicated an early indication of possible stimulation by TFAM. There is an increase in the product formed from 0.2 µM to 0.5 µM up to 26.25% product formed for the 400 nM AAG trial. However, for the 200 nM trial, the peak is seen around 0.5 µM at 8.75 µM. This makes sense as there is more enzyme in the 400 nM trial and therefore more product is formed. After 1 µM TFAM concentration, the product formed

seems to drop below the control AAG only point at 0 µM TFAM concentration. This could indicate that TFAM potentially has inhibiting effects at higher concentrations. There is significantly lower product formation for

a.

TFAM Concentration (µM) with 200 nM AAG	% Product Formed
DNA	5.83
Only AAG	5.84
0.2	7.24
0.5	8.75
1.0	3.03
2.0	0.19
TFAM Concentration (µM) with 400 nM AAG	
Only AAG	15.88
0.2	26.25
0.5	26.12
1.0	9.91
2.0	3.94

b.

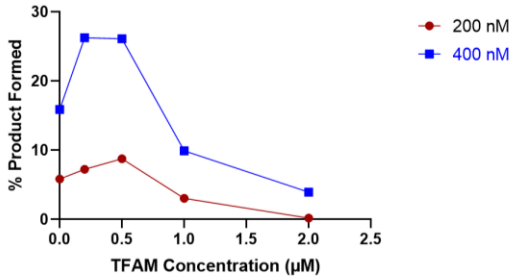

c.

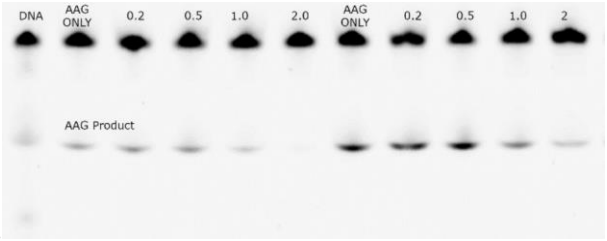

Figure 3. 3a. Percent product of AAG formed for each TFAM concentration. 3b. Graph indicating AAG+TFAM behavior at different concentrations. 3c. Visualization of assay through a 16% Gel.

both the 200 nM and 400 nM concentrations after 1.0 µM. With this consideration the second optimization assay was done only for a range up to 1.2 µM rather than 2.0 µM. This also allowed for extra points to be added at smaller concentrations for a clearer picture of where this possible stimulation was occurring. This optimization assay included additional points at 0.2, 0.3, and 1.2 µM TFAM concentrations. Similar to the last experiment, at lower concentrations an increase of AAG product formation is seen, while a slight inhibition of product formation is visualized after 1.0 µM. Both gel images indicated darker bands at the lower concentrations and gradually decreased as the concentration of TFAM increased. As with the last optimization assay, the 400 nM reaction was producing much more product, and therefore had more glycosylase activity compared to the 200 nM, likely due to the increase in enzyme available to react. This is consistent with the first optimization assay. Furthermore, consistent with the first assay, the 400

nM AAG concentration provided a much clearer depiction of the results due to the high concentration of AAG. The 200 nM results indicated a slight increase in product seen broadly across points from 0.1 µM to 0.5 µM until a drop in product formation is seen. Meanwhile, the 400 nM AAG concentration shows a much more drastic increase in product formation with the peak product formed at 0.3 µM TFAM concentration with 23.25% product produced, and a gradual decrease in product after 0.5 µM. Considering this, the following experiments are all done in 400 nM AAG concentration for the best visualization of AAG and TFAM interaction at lower concentrations of TFAM. Now that the assay had been optimized, a smaller range of TFAM concentration was chosen, 0.1 µM to 1.0 µM for the following experiments. This ensured a point at intervals of 0.1 µM concentration up to 1.0 µM of TFAM concentration. As previously

a. 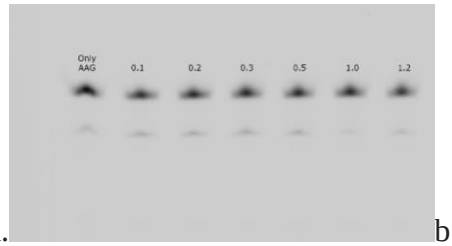

b. 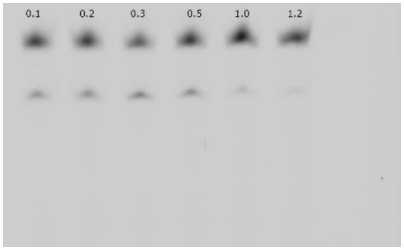

c.

TFAM Concentration (µM)	% Product Formed
0 – Only AAG Blank	5.76
0.1	9.09
0.2	7.24
0.3	8.66
0.5	7.5
1.0	2.56
1.2	4.63

d.

TFAM Concentration (µM)	% Product Formed
0 – Only AAG Blank	5.76
0.1	15.43
0.2	16.55
0.3	23.25
0.5	15.24
1.0	3.99
1.2	2.49

Figure 4. Optimization assay with TFAM range of 0.1 µM to 1.2 µM. 4a,b. Visualization of assay using gel. 4c,d. Table of percent product formed for 200 nM and 400 nM AAG concentrations, respectively. 4e,f. Graphical visualization of AAG behavior in the presence of TFAM.

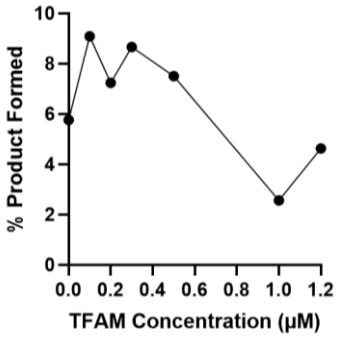

e.

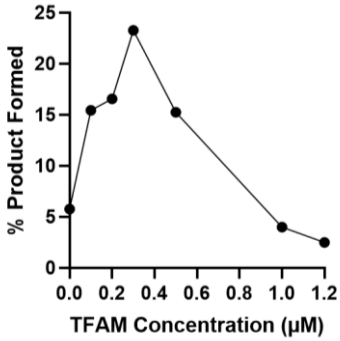

f.

mentioned, the 400 nM concentration of AAG is used for the best visualization of the impact of TFAM on AAG glycosylase activity. The proceeding assay is run with 12 points, 2 of which are control. It was seen in the results of this assay that as previously seen with the optimization results, there is a slight increase in the product formation of 400 nM AAG at lower concentrations of TFAM. When examining the gel image, you can see a slight increase in the darkness, and therefore the content in the bands in the lower concentrations versus the concentrations after 0.5 and 0.6 μM, which was consistent on both trials of the gel. In this assay, the only DNA lane stands as a control to compare the rest of the results against. The only AAG lane stands as another control to compare the rest of the lanes against. As previously mentioned, lane 2 is used to as a base to compare the product formation at the rest of the concentrations of TFAM, to see if there is an increase in product when AAG is added to a TFAM-DNA complex mixture, or whether there is inhibition of product formation, as well as no change. When visualizing the data as a graph, from 0.1 μM to 0.5 μM, there is a consistent increase in the product being formed. However, these results do not indicate a spike in product formation at any similar points, rather it is a general increase in percent product which is consistent until 0.5 μM of TFAM, after which, a decrease in percent product formation is seen. This trend of increase in

percent product formed at lower concentrations and then a gradual decrease from about 0.5 µM TFAM concentration has been

a.

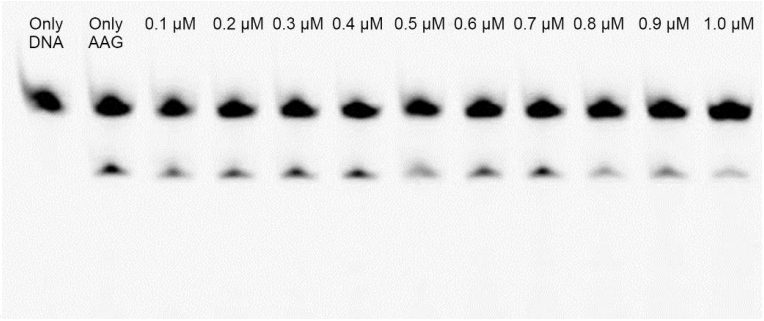

b.

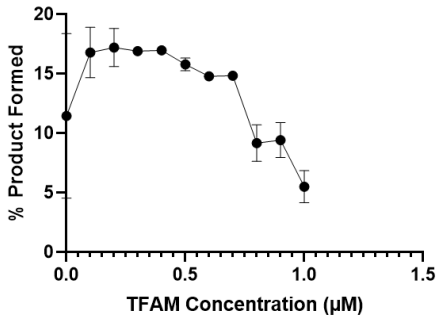

Figure 5. 10-point assay of TFAM-AAG assay with 400 nM AAG. 5a. Gel image of trial visualizing results from the assay. Darker bands indicate more product. 5c. Graphical visualization of results. Increase in % product formed seen from 0.1 µM to 0.5 µM. Error bars indicate standard deviation between two trials.

consistent so far in both the optimization assay and the TFAM-AAG assay with 400 nM of AAG. The decrease in product seen after 0.5 µM, and specifically at much higher concentrations of TFAM, such as 0.8 to 1.0 µM, also possibly indicates an inhibition of glycosylase product formation (figure 5b). The percent product formed at those higher concentrations reaches below the control percent product formed. The control data point has only AAG within the reaction, so it is not competing with TFAM to bind and function. Therefore, it should theoretically form the product as the glycosylase normally would. This is why when there is an increase in product formation at the lower points, we can estimate a stimulating effect by TFAM. However, with the higher concentration points, when the percent product formed drops below the control, we can estimate a possible inhibiting impact of TFAM binding to the dsDNA. In all, this data indicates

that TFAM likely slightly stimulates the percent product formation of AAG at a very small concentration of TFAM before gradually decreasing to the point of almost inhibition of product formation (figure 5).

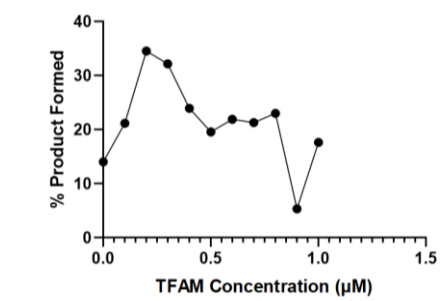

a.

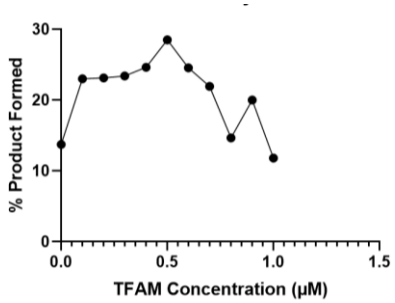

b.

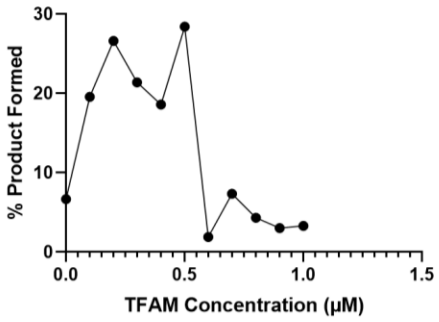

c.

Figure 6. Multiple graphical analysis of TFAM-AAG assay results. Each graph correlates to a separate trial. All points and conditions are kept consistent throughout all trials, and with previously mentioned results.

Multiple experiments were conducted to test for reproducibility. Similar to the aforementioned results, data collected from technical trials showed a relatively similar product formation trend with an increase in product formation compared to the control (only AAG) reaction mixture. Results from these trials do not indicate specific single points of significant stimulation, with the exception of results in Figure 6c. There seems to be significant product formation in that specific trial, which could be a result of technical error. However, the general trend of product formation remains consistent throughout the trials. Generally, there is an increase in product formation that

remains between 20 to 28% of products formed. This is consistent throughout the different trials of the assay.

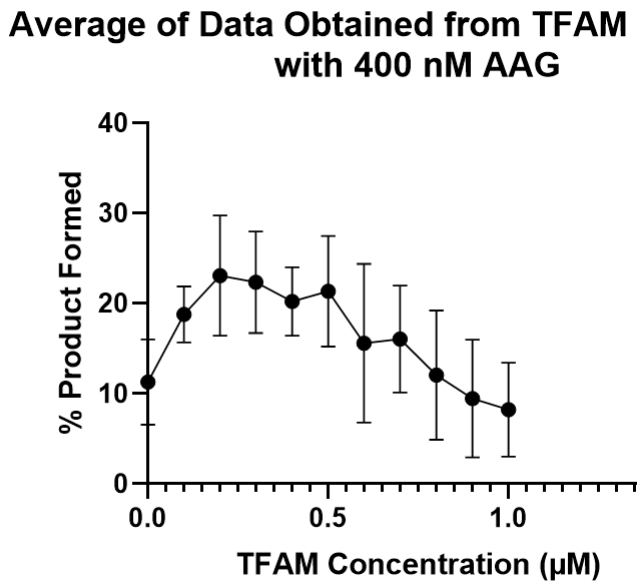

Figure 7. The average of all of the trials producing data for AAG-TFAM assay. Up to 7 trials per data point, including points from optimization assay using 400 nM AAG. The error bars indicate the standard deviation between the results of each point from different trials.

0, 0.2, 0.5, 1.0 µM data points include data from 7 different trials (optimization trials included). 0.3, 0.5 µM from 6 trials (optimization trials included). 0.4, 0.6-0.9 µM include data from 5 trials.

Throughout the project, multiple trials, as previously mentioned, were conducted and data were recorded for each. Figure 7 illustrates the visualization of the data from the average of 7 different trials. Each data point on this graph represents up to 7 different raw data points from different trials. The error bars indicate the standard deviation between the different results at each concentration of each point. Data points at 0 µM, 0.2 µM, 0.5 µM, and 1.0 µM are averages of data from 7 different trials, including the optimization data. Data points at 0.1 µM, and 0.3 µM contain data from 6 different trials, also including optimization data. Data points at 0.4 µM, and 0.6 µM through 0.9 µM contain data from 5 different trials, these do not include data from optimization assays, as these points were not included in the assay. By averaging the data from optimization, and technical trials together, the graph provides an overall, generalized visual of the results from the TFAM-AAG assay. In these results, an increase in the percent product formation is seen at lower concentrations from 0.1 to 0.5 µM, while a gradual decrease is visible

in the latter concentrations of TFAM. Although the product formation is not considerable enough to determine if the TFAM-DNA complex in the reaction is indeed causing a stimulating effect at lower concentrations, it does show that it does not begin complete inhibition of the glycosylase activity until higher concentration levels of TFAM are reached. The average of the data collected is certainly consistent overall with the individual results listed in this thesis. Results have indicated a slight increase in AAG product formation at smaller concentrations of TFAM when AAG is introduced to TFAM complexed DNA, followed by a slight decline.

Discussion

Impact on AAG product formation by TFAM. Considering that both TFAM and AAG are localized in the mitochondrial DNA region, it was to be expected that the proteins likely interacted with each other, or complexed forms of the other. Therefore, the purpose of the project was to study the impact of TFAM on AAG binding and subsequent glycosylase activity. Results have indicated that although not too significant, there is still some impact that the TFAM-DNA complex has on the glycosylase activity of AAG. In Figure 7, where the average of all of the trial data is visualized graphically, the takeaway is that there is still a small amount of increase in product formation at lower concentrations of TFAM, however, at higher concentrations the effect gradually changes to an almost inhibiting activity. Initial optimization assays had shown a spike in the product formation at low concentrations which was significant to be considered a stimulating effect by TFAM. However, these assays were done with a small number of points at those lower concentrations (2 to 3 points between 0.1 µM and 0.5 µM), therefore it is possible that these optimization assays were not giving a detailed idea of the enzyme activity. Further detailed trials with 10 points ranging from 0.1 µM to 1.0 µM, provided evidence of a slight

increase in AAG glycosylase activity, however, not one that was significant. This increase was also gradual and maintained until the 0.6 μM point was reached.

Expected outcomes vs. Actual. Data from work in our laboratory had indicated that the glycosylase activity of another protein, Uracil-DNA Glycosylase-1(UNG1), was stimulated when interacting with a TFAM-complexed DNA. Based on this preliminary data, we suspected a similar case with AAG's glycosylase activity. Similarities between UNG1 and AAG prompted the presumption that similar results will be seen. For example, both proteins initiate the BER pathway, and both are glycosylases. AAG has a rate-limiting step in multiple-turnover kinetics as the dissociation of its product (Hedglin et. al., 2008). UNG1 also has its rate-limiting step at the dissociation of its abasic product (Bharati et. al., 1998). These similarities and the optimization assays, as previously mentioned, also hinted towards TFAM stimulation with AAG, and therefore expected outcome was that we would see a significant stimulating impact by TFAM concentrations on AAG product formation. However, results indicated that the increase in product formation was not as significant as previously thought. This could likely be a result of the inherent differences between the chemistry and structure of the proteins AAG and UNG1. For example, although both AAG and UNG1 are glycosylases that initiate the base excision repair pathway, their choice of substrate differences stands out. AAG targets alkyl adenines, or purines specifically and structure and function are critically linked (Hedgelin et. al., 2008). Meanwhile, UNG1 targets uracil, a pyrimidine, which is chemically and sterically different from purines (Sarno et. al., 2019). Therefore, although significant stimulation was expected, the actual results indicated a smaller increase in product formation before a gradual decline into an inhibiting effect at higher concentrations of TFAM. Therefore, it cannot be confidently said that AAG is indeed impacted by TFAM through a stimulating effect.

Impact of the relationship between TFAM and AAG. DNA damage can be detrimental to the survival of the mitochondria and the cell. Whether TFAM has a stimulating effect, inhibiting effect, or no effect on the glycosylase ability of AAG is likely to play a role in the long-term survivability of the mitochondria. Therefore, gaining the understanding that at higher concentrations of TFAM, a gradual inhibition of AAG product formation is seen offers valuable insight into the behavior of each enzyme in the presence of the other. Recent studies have shown that damage to mitochondrial DNA, similar to the ones which glycosylase such as AAG repair, have been associated with metabolic pathologies, cancers, and neurodegenerative diseases (Sharma, et. al., 2019). Furthermore, accumulation of damage to the mitochondrial DNA has been correlated with diseases related to age (Sharma et. al., 2019). It comes as no surprise then, the importance of studying glycosylases and understanding their impact, or lack thereof, on DNA repair. By learning the impact TFAM may have on AAG, it may have lasting implications in many fields of study, including therapeutic development for the aforementioned diseases.

Conclusion

In summary, the result from my data indicates the ability of TFAM to allow for AAG product formation at lower TFAM concentrations. Data indicates that at much higher concentrations of TFAM, and therefore, TFAM-DNA complex, there is inhibition of AAG product formation. Although the data was not exactly what was expected, which was a much more significant impact of TFAM, the results still provided more insight into the relationship between TFAM and AAG than before. The science and techniques behind studying enzymes are important and impactful. Future steps in this research may involve testing the glycosylase activity of AAG with TFAM using a variety of different substrate DNAs. Understanding the effect of these competing enzymes with different substrates may help gain a clearer

understanding of their behaviors. Continued study of the relationship between TFAM and AAG will allow for a much better understanding of the mitochondrial DNA region and its maintenance. With optimism, continued research focusing on glycosylase activity may have impactful, and beneficial improvements in our understanding of the human system, and developments in medicine.

REFERENCES

Atig, R. Kefi-Ben, et al. “Mitochondrial DNA: properties and applications.” *Archives de l’Institut Pasteur de Tunis*, vol. 86, no. 1–4, 2009, pp. 3–14.

Bharati, S., et al. “Human Mitochondrial Uracil-DNA Glycosylase Preform (UNG1) Is Processed to Two Forms One of Which Is Resistant to Inhibition by AP Sites.” *Nucleic Acids Research*, vol. 26, no. 21, 1998, pp. 4953–4959, https://doi.org10.1093/nar/26.21.4953.

Chandrasekaran, Krish, et al. “Role of Mitochondria in Diabetic Peripheral Neuropathy: Influencing the NAD+-Dependent SIRT1-PGC-1α-TFAM Pathway.” *International Review of Neurobiology*, vol. 145, 2019, pp. 177–209, https://doi.org10.1016/bs.irn.2019.04.002.

Hedglin, Mark, and Patrick J. O’Brien. “Human Alkyladenine DNA Glycosylase Employs a Processive Search for DNA Damage.” *Biochemistry*, vol. 47, no. 44, 2008, pp. 11434–11445, https://doi.org10.1021/bi801046y.

Jacobs, Angelika L., and Primo Schär. “DNA Glycosylases: In DNA Repair and Beyond.” *Chromosoma*, vol. 121, no. 1, 2012, pp. 1–20, https://doi.org10.1007/s00412-011-0347-4.

Kennedy, Erin E., et al. “Global Repair Profile of Human Alkyladenine DNA Glycosylase on Nucleosomes Reveals DNA Packaging Effects.” *ACS Chemical Biology*, vol. 14, no. 8, 2019, pp. 1687–1692, https://doi.org10.1021/acschembio.9b00263.

Sampath, Harini, et al. “Regulation of DNA Glycosylases and Their Role in Limiting Disease.” *Free Radical Research*, vol. 46, no. 4, 2012, pp. 460–478, https://doi.org10.3109/10715762.2012.655730.

Sarno, Antonio, et al. “Uracil-DNA Glycosylase UNG1 Isoform Variant Supports Class Switch Recombination and Repairs Nuclear Genomic Uracil.” *Nucleic Acids Research*, vol. 47, no. 9, 2019, pp. 4569–4585, https://doi.org10.1093/nar/gkz145.

Xu, Wenyan, et al. “Mitochondrial Transcription Factor A Promotes DNA Strand Cleavage at Abasic Sites.” *Proceedings of the National Academy of Sciences of the United States of America*, vol. 116, no. 36, 2019, pp. 17792–17799, https://doi.org10.1073/pnas.1911252116.